



Effects of the slip boundary condition on dynamics and pull-in instability of carbon nanotubes conveying fluid

Himan Rashidi¹ · Zaher Rahimi¹ · Wojciech Sumelka²

Received: 20 June 2018 / Accepted: 27 October 2018 / Published online: 2 November 2018
© The Author(s) 2018

Abstract

This paper addresses the effects of the slip boundary condition on dynamics and pull-in instability of carbon nanotubes (CNTs) containing internal fluid flow. Both the clamped–clamped and the cantilever boundary conditions are considered. The structure of CNTs is modelled using the size-dependent strain gradient theory (SGT) of continuum mechanics. It is shown that the Knudsen number (Kn) has a significant effect on the static and dynamic CNT response due to pull-in voltage loading and the existence of the instability region.

1 Introduction

CNTs attract much attention nowadays due to their superior mechanical, thermal and electrical properties and also their numerous applications (Iijima 1991; Yamamoto et al. 2012; Umeda et al. 2012; Xu et al. 2012; Che et al. 1998; Evans et al. 1996). A remarkable number of studies in this field have been conducted, especially concerning the fluid–structure interaction. For instance, Yoon et al. (2005) studied free vibration and instability of CNTs with internal fluid. Wang et al. (2008) investigated buckling instability considering the effect of the Van der Waals force, and Zhang and Fang (Zhen and Fang 2010) presented the thermal and nonlocal effects on vibration for both CNT and the conveyed fluid. The aspect ratio, the viscosity effect and elastic medium parameters, as well as the nonlocal effect, were considered by Chang and Lee (2009). Kaviani and Mirdamadi (2013) studied the wave propagation phenomena in CNTs with internal fluid, using the strain/inertia gradient theory and considering the slip boundary condition and Knudsen number in the solid–fluid interaction. Furthermore, in Kaviani and Mirdamadi (2012), they presented the effect of Kn and the slip boundary condition coupling on the viscosity of the nanofluid which passes through a CNT.

Generally, we can distinguish the following regimes of flow (Kaviani and Mirdamadi 2012; Mirramezani and Mirdamadi 2012; Kucaba-Piętal 2004): (1) $0 < Kn < 10^{-2}$ for the continuum flow regime; (2) $10^{-2} < Kn < 10^{-1}$ for the slip flow regime; (3) $10^{-1} < Kn < 10$ for the transition flow regime; and (4) $Kn > 10$ for the free molecular flow regime. In this paper, we consider the interval $0 < Kn < 10^{-1}$. It contains both the continuum and the slip flow regimes. From the point of view of modelling, the commonly known governing equations for the conventional fluid–structure interaction problems result from the assumption of no-slip boundary conditions. However, if we consider the influence of Kn on the CNT behaviour, this condition is no longer valid. Therefore, we have to use the conventional Navier–Stokes equations satisfying the slip boundary conditions on the tube walls and then find out an average velocity correction factor that relates the average velocity of the no-slip and the slip boundary conditions to each other.

The effects of the slip and no-slip boundary conditions, and Kn can be found in the literature. Kaviani et al. (Kaviani and Mirdamadi 2012) studied the effects of Kn and the slip boundary condition for a nanoflow passing through a nanotube. Mirramezani et al. (Mirramezani and Mirdamadi 2012a, b) studied vibrational behaviour of CNTs considering small-size effects for both the slip boundary condition on fluid flow and the solid structure using the Euler–Bernoulli plug flow theory. Wave propagation of CNTs conveying fluid was studied by Kaviani et al. (Kaviani and Mirdamadi 2013) in which the slip boundary condition was considered based on the gradient theory of continuum mechanics. Mirramezani et al. (2013) proposed a new model for 1D coupled

✉ Zaher Rahimi
st_z.rahimi@urmia.ac.ir

¹ Department of Mechanical Engineering, Urmia University, Urmia, Iran

² Institute of Structural Engineering, Poznan University of Technology, Piotrowo 5 Street, 60-965 Poznan, Poland

vibrations of CNTs conveying fluid in which they took into account the slip boundary condition using Kn and the size-dependent continuum theories.

Research in nanotechnology is often multidisciplinary. For instance, the study of micro/nanoelectromechanical systems (MEMS and NEMS) is an important research area which includes the concepts of basic sciences as well as mechanical and electrical engineering. The most effective and applicable technique to actuate NEMS is the electrostatic actuation method (Fakhrabadi et al. 2013). Dequesnes et al. (2002, 2004) investigated the deflection and the static pull-in of CNTs under electrostatic actuation considering the Van der Waals force. Rasekh and Khadem (Rasekh et al. 2010) studied the static and dynamic behaviour of CNTs under the electrostatic and Van der Waals force. Ouakad and Younis (2010) studied the nonlinear dynamics of CNTs with the clamped–clamped and the cantilever boundary conditions under DC and AC electrical excitations. Hajnayeb et al. (Hajnayeb and Khadem 2012) presented forced vibration of a double-wall CNT under the axial force and AC–DC complex electrostatic actuations. Fakhrabadi et al. (2013) investigated the influence of the fluid flow on static and dynamic behaviour of electrostatically actuated CNTs with cantilever and doubly clamped boundary conditions, using SGT. More recently, some researchers have studied the vibration and instability of nano- and micro-tubes conveying fluid (Ghazavi and Molki 2018; Guo et al. 2018; Zhang et al. 2017, 2016; Wang et al. 2016).

The main purpose of this paper is to study the effects of the slip and no-slip boundary conditions on the pull-in instability and dynamics of the clamped–clamped and the cantilever CNTs conveying fluid, utilizing the SGT, to consider the small-scale effect of the nano-structure. The value of Kn is in the interval $0 < Kn < 10^{-1}$, which includes the slip boundary conditions on the CNT wall. We show the effect of the fluid velocity on the static and dynamic pull-in instability in the presence of different values of Kn . Finally, we study the effects of the slip and no-slip boundary conditions on the flutter (dynamic instability) and the buckling (static instability) of the CNTs under the electrostatic force.

2 System description and mathematical formulation

We consider a fluid conveying CNT (Fig. 1). The CNT is clamped over a metal plate with an initial gap (G_0). A potential difference (V) is applied to the CNT (the positive electrode) and the metal plate (the negative electrode). Thus, the CNT is subjected to an electrostatic distributed load. Generally, the value of this electrostatic force is associated with the deflections of the CNT. The deflection corresponds to the applied voltage as long as the elastic force of the CNT can balance the

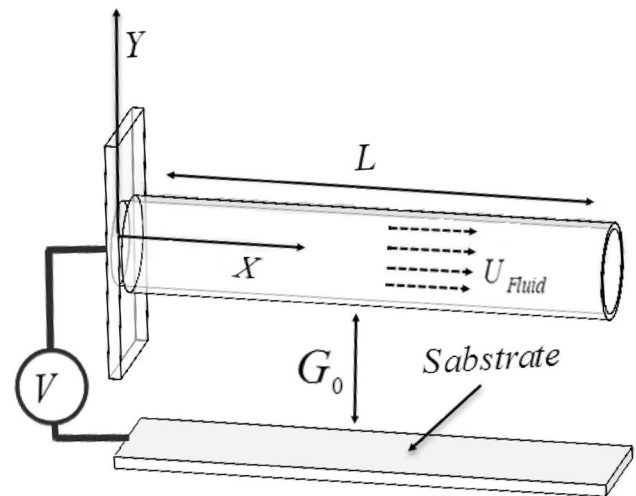


Fig. 1 A schematic diagram of electrostatically actuated CNTs conveying fluid

attractive force resulting from the applied voltage. However, at some point the tip of the cantilevered CNT or the centre of the doubly clamped CNT suddenly drops on the metal plate. This phenomenon is called pull-in instability and the corresponding voltage is called the pull-in voltage.

Since the classical elasticity theory often fails to predict the mechanical behaviour of the micro/nanostructures precisely, some researchers have tried to develop non-classical elasticity theories to enhance the accuracy and capability of numerical modelling techniques to predict of desired behaviour. According to the SGT, the strain energy U of an isotropic linear elastic material with volume Ω under an infinitesimal deformation can be formulated as follows (Kahrobaiyan et al. 2011):

$$U_s = \frac{1}{2} \int \int \int_{\Omega} \left(\sigma_{ij} \varepsilon_{ij} + P_i \gamma_j + \tau_{ijk}^{(1)} \eta_{ijk}^{(1)} + m_{ij}^s \chi_{ij}^s \right) dV, \quad (1)$$

where ε_{ij} , γ_j , $\eta_{ijk}^{(1)}$, χ_{ij}^s denote components of the strain tensor, P is the dilatation gradient vector, γ is the deviatoric stretch, η_1 the gradient tensor, and χ^s is the symmetric part of the rotation gradient tensor. They are defined by the following relations:

$$\varepsilon_{ij} = \frac{1}{2} (\partial_i u_j + \partial_j u_i), \quad (2)$$

$$\eta_{ijk}^{(1)} = \frac{1}{3} (\partial_i \varepsilon_{jk} + \partial_j \varepsilon_{ki} + \partial_k \varepsilon_{ij}) - \frac{1}{15} [\delta_{ij} (\partial_k \varepsilon_{mm} + 2\partial_j \varepsilon_{mk}) + \delta_{jk} (\partial_i \varepsilon_{mm} + 2\partial_m \varepsilon_{mi}) + \delta_{ki} (\partial_j \varepsilon_{mm} + 2\partial_m \varepsilon_{mj})], \quad (3)$$

$$\gamma_i = \partial_i \varepsilon_{mm}, \quad (4)$$

$$\chi^s_{ij} = \frac{1}{2}(e_{ipq}\partial_p \epsilon_{qj} + e_{jpr}\partial_r \epsilon_{qi}), \tag{5}$$

$$\theta_i = \frac{1}{2}[\text{curl}(u)]_i, \tag{6}$$

where u_i, θ_i denote the components of the displacement vector and infinitesimal rotation vector, respectively. The conjugated force parameters for $\epsilon, \gamma, \eta^{(1)}$ and χ^s are denoted by $\sigma, P, \tau^{(1)}$ and m^s , respectively, where the first one is the classical stress tensor and the next ones are the higher order stresses. They are defined as follows (Kahrobaiyan et al. 2011):

$$\sigma_{ij} = \lambda \text{tr}(\epsilon)\delta_{ij} + 2G\epsilon_{ij}, \tag{7}$$

$$p_i = 2l_0^2 G \gamma_j, \tag{8}$$

$$\tau_{ijk}^{(1)} = 2l_0^2 G \eta_{ijk}^{(1)}, \tag{9}$$

$$m_{ij} = 2l_2^2 G \chi_{ij}, \tag{10}$$

where λ and μ are Lamé’s constants and l_0, l_1, l_2 are the material length scale parameters corresponding to the dilatation gradient, the deviatoric stretch gradient and the rotation gradient, respectively. Substituting Eqs. (7–10) into Eq. (1), applying the Hamilton principle and using some mathematical calculations, we obtain the equation of motion of the CNT (Fakhrabadi et al. 2014):

$$S \frac{\partial^4 w}{\partial x^4} - K \frac{\partial^6 w}{\partial x^6} - N \frac{\partial^2 w}{\partial x^2} + m \frac{\partial^2 w}{\partial t^2} + c \frac{\partial w}{\partial t} = q(x, t), \tag{11}$$

where

$$S = EI + GA \left(2l_0^2 + \frac{120}{225} l_1^2 + l_2^2 \right), \tag{12}$$

$$K = GI \left(2l_0^2 + \frac{4}{5} l_1^2 \right), \quad m = \rho A, \tag{13}$$

$$N = N_0 + \frac{EA}{2L} \int_0^L \left(\frac{\partial w}{\partial x} \right)^2 dx, \tag{14}$$

$$q(x, t) = q_{\text{fluid}} + q_{\text{elec}}, \tag{15}$$

and $E, I, G, A, w, x, N, c, L,$ and t are elastic modulus, moment of inertia, shear modulus, cross-sectional area, deflection, axial coordinate, axial force, damping coefficient, length of the CNT, and time, respectively.

Next, we define the boundary conditions for cantilever and doubly clamped CNTs with Eqs. (16) and (17), respectively:

$$\begin{aligned} w(0, t) = \frac{\partial w(0, t)}{\partial x} = \frac{\partial^2 w(0, t)}{\partial x^2} = 0, \\ -K \frac{\partial^5 w(L, t)}{\partial x^5} + S \frac{\partial^3 w(L, t)}{\partial x^3} = 0, \\ -K \frac{\partial^4 w_i(L, t)}{\partial x^4} + S \frac{\partial^2 w(L, t)}{\partial x^2} = 0, \end{aligned} \tag{16}$$

$$K \frac{\partial^3 w(L, t)}{\partial x^3} = 0,$$

$$\begin{aligned} w(0, t) = \frac{\partial w(0, t)}{\partial x} = \frac{\partial^2 w(0, t)}{\partial x^2} = 0, \\ w(L, t) = \frac{\partial w(L, t)}{\partial x} = \frac{\partial^2 w(L, t)}{\partial x^2} = 0. \end{aligned} \tag{17}$$

The distributed external force in Eq. (11) comprises the electrostatic force and the force which results from the fluid flow through the CNT.

The electrostatic force can be written as (Dequesnes et al. 2002)

$$q_{\text{elec}} = \frac{\pi \epsilon_0 V^2}{\sqrt{(G_0 - w)(G_0 - w + 2R)} \arccos h^2 \left(1 + \frac{G_0 - w}{R} \right)}, \tag{18}$$

where ϵ_0, V, R and G_0 represent the electrical permittivity of the vacuum ($= 8.854$ PF), voltage, the radius of the CNT and the initial gap, respectively.

The force resulting from the fluid flow including the slip boundary condition can be obtained as follows:

We follow the considerations by Beskok and Karniadakis (1999). Within this model, the equation based on experimental data is postulated in the following form:

$$U_s - U_w = \left(\frac{2 - \sigma_v}{\sigma_v} \right) \left(\frac{Kn}{1 - bKn} \right) \left(\frac{\partial U}{\partial n} \right)_{r=R}, \tag{19}$$

where b is a general slip coefficient. Choosing $b = -1, U_s$ is the slip velocity of the fluid near the CNT wall surface, U_w is the axial rigid body solid wall velocity, and n is the outward unit vector normal to the CNT wall surface. The parameter σ_v is the tangential momentum accommodation coefficient and is assumed to be 0.7 for practical purposes (Shokouhmand et al. 2010).

In this paper, Eq. (19) is used to model the slip velocity boundary condition in the Navier–Stokes equations. Up to now, for conventional FSI problems, no-slip boundary conditions were considered, in which the influence of Kn on CNTs was not included. Thus, the conventional Navier–Stokes equations are used but the slip boundary conditions on the tube walls are satisfied and an average velocity correction

factor is established, which relates to the average velocity of the no-slip and slip boundary conditions.

Therefore, a fully developed, incompressible, viscous fluid flow of constant density and viscosity is considered. Since the Newtonian fluid with a constant pressure gradient and negligible effect of gravitational body force is taken into account, the Navier–Stokes equations are (Shames 1962):

$$\rho \frac{D\vec{U}}{Dt} = -\nabla P + \mu \nabla^2 \vec{U} + \vec{F}_{\text{body}}, \tag{20}$$

where ρ is the mass fluid density, P is pressure, and $\frac{D}{Dt}$ is the material derivative. In the slip regime, the effective viscosity of the fluid is considered, which, according to Beskok and Karniadakis model (Beskok and Karniadakis 1999) is:

$$\begin{aligned} \mu_e &= \mu Cr(Kn), \\ Cr &= \left(\frac{1}{1 + \alpha Kn} \right), \end{aligned} \tag{21}$$

where the coefficient α can vary from zero to a constant value, according to the formula (Karniadakis et al. 2006):

$$\alpha = \alpha_0 \frac{2}{\pi} \left[\tan^{-1}(\alpha_1 Kn^B) \right], \tag{22}$$

where $\alpha_1 = 4$ and $B = 0.04$ are experimental data and α_0 can be obtained from the free molecular regime:

$$\lim_{Kn \rightarrow \infty} \alpha = \alpha_0 = \frac{64}{3\pi \left(1 - \frac{4}{b} \right)}. \tag{23}$$

The solution of Eq. (20) in the axial direction of cylindrical orthogonal coordinates is (Shames 1962):

$$U = \frac{1}{4\mu_e} \left(\frac{\partial p}{\partial x} \right) r^2 + C. \tag{24}$$

Hence, to obtain C , we use Eq. (19):

$$U_{r=R} = -R \left(\frac{2 - \sigma_v}{\sigma_v} \right) \left(\frac{Kn}{1 - bKn} \right) \left(\frac{\partial U}{\partial n} \right)_{r=R}, \tag{25}$$

where R is the inner radius of the CNT. Substituting Eq. (25) into Eq. (26) leads to the slip and no-slip velocities:

$$\begin{aligned} U_{\text{slip}} &= \frac{1}{4\mu_0 Cr(Kn)} \left(\frac{\partial p}{\partial x} \right) \left[r^2 - R^2 - 2R^2 \left(\frac{2 - \sigma_v}{\sigma_v} \right) \left(\frac{Kn}{1 - bKn} \right) \right], \\ U_{\text{no-slip}} &= \frac{1}{4\mu_0} \left(\frac{\partial p}{\partial x} \right) (r^2 - R^2). \end{aligned} \tag{26}$$

The VCF coefficients are defined as follows:

$$\text{VCF} = \frac{U_{\text{avg-slip}}}{U_{\text{avg-noslip}}} = \frac{1}{Cr(Kn)} \left(4 \left(\frac{2 - \sigma_v}{\sigma_v} \right) \left(\frac{Kn}{1 - bKn} \right) + 1 \right). \tag{27}$$

Finally, the following equation for external force due to the fluid flow is obtained (Wang and Ni 2009):

$$\begin{aligned} q_{\text{fluid}} &= \left[m_f(\text{VCF})^2 U_{\text{avg-noslip}}^2 + P^* A \right] \frac{\partial^2 w}{\partial x^2} - 2m_f(\text{VCF}) U_{\text{avg-noslip}} \frac{\partial^2 w}{\partial x \partial t} \\ &\quad - m_f \frac{\partial^2 w}{\partial t^2} + \mu(Cr) A_i \frac{\partial^3 w}{\partial x^2 \partial t} + \mu(Cr)(\text{VCF}) U_{\text{avg-noslip}} A_i \frac{\partial^3 w}{\partial x^3}, \end{aligned} \tag{28}$$

where m_f , P^* , m_c , μ and A_i represent the fluid mass, fluid pressure, mass of the CNT per unit length, fluid viscosity and fluid cross-section, respectively. Substituting Eqs. (28) and (18) into Eq. (11) leads to the equation of motion of a CNT conveying fluid:

$$\begin{aligned} S \frac{\partial^4 w}{\partial x^4} - K \frac{\partial^6 w}{\partial x^6} + \left(m_f(\text{VCF})^2 U_{\text{avg-noslip}}^2 + P^* A - N \right) \frac{\partial^2 w}{\partial x^2} \\ + 2m_f(\text{VCF}) U_{\text{avg-noslip}} \frac{\partial^2 w}{\partial x \partial t} + (m_c + m_f) \frac{\partial^2 w}{\partial t^2} - \mu(Cr) A \frac{\partial^3 w}{\partial x^2 \partial t} \\ - \mu(Cr) A (\text{VCF}) U_{\text{avg-noslip}} \frac{\partial^3 w}{\partial x^3} + c \frac{\partial w}{\partial t} = q_{\text{elec}}, \end{aligned} \tag{29}$$

where $(P^* A - N) \frac{\partial^2 w}{\partial x^2}$ is equal to zero for the CNTs.

3 Solution

We define the following non-dimensional parameters:

$$\begin{aligned} \hat{w} &= \frac{w}{G_0}, \quad \hat{x} = \frac{x}{G_0}, \quad \hat{R} = \frac{R}{G_0}, \\ \hat{t} &= \frac{t}{t^*}, \quad t^* = \sqrt{\frac{(m_c + m_f)L^4}{EI}}, \\ u_{\text{avg}} &= \left(\frac{m_f}{EI} \right)^{\frac{1}{2}} LU_{\text{avg}}. \end{aligned} \tag{30}$$

Substituting the above non-dimensional parameters into Eq. (30), we have:

$$\begin{aligned} \frac{\partial^4 \hat{w}}{\partial \hat{x}^4} - \alpha_1 \frac{\partial^6 \hat{w}}{\partial \hat{x}^6} + \alpha_2 \frac{\partial^2 \hat{w}}{\partial \hat{x}^2} + \beta \frac{\partial^2 \hat{w}}{\partial \hat{x} \partial \hat{t}} + \gamma \frac{\partial^2 \hat{w}}{\partial \hat{t}^2} - \delta \frac{\partial^3 \hat{w}}{\partial \hat{x}^2 \partial \hat{t}} \\ - \xi \frac{\partial^3 \hat{w}}{\partial \hat{x}^3} + \zeta \frac{\partial \hat{w}}{\partial \hat{t}} = \alpha \hat{q}_{\text{elec}}, \end{aligned} \tag{31}$$

where the lateral displacement $w(\hat{x}, \hat{t})$ consists of a static part and a dynamic part:

$$\hat{w}(\hat{x}, \hat{t}) = \hat{w}_s(\hat{x}) + \hat{w}_d(\hat{x}, \hat{t}). \tag{32}$$

3.1 Static analysis

Ignoring the inertia terms in Eq. (31), the static equation is represented by the relation:

$$\frac{\partial^4 \hat{w}_s}{\partial \hat{x}^4} - \alpha_1 \frac{\partial^6 \hat{w}_s}{\partial \hat{x}^6} + \alpha_2 \frac{\partial^2 \hat{w}_s}{\partial \hat{x}^2} - \xi \frac{\partial^3 \hat{w}_s}{\partial \hat{x}^3} = \alpha \hat{q}_{elec}(V, \hat{w}). \tag{33}$$

To solve the above equation, we use the step-by-step linearization method (SSLM) (Talebian et al. 2010), where the voltage and the deflection in the K th step are V_K and \hat{w}_K , and in the $(K + 1)$ th step V_{K+1} and \hat{w}_{K+1} . The resultant deflections in the $(K + 1)$ th step can be written as

$$V^{i+1} = V^i + \delta V, \tag{34}$$

$$\hat{w}_s^{i+1} = \hat{w}_s^i + \delta \hat{w} = \hat{w}_s^i + \psi(\hat{x}).$$

Hence, for the $(K + 1)$ th step, Eq. (33) can be rewritten as

$$\frac{\partial^4 \hat{w}_s^{K+1}}{\partial \hat{x}^4} - \alpha_1 \frac{\partial^6 \hat{w}_s^{K+1}}{\partial \hat{x}^6} + \alpha_2 \frac{\partial^2 \hat{w}_s^{K+1}}{\partial \hat{x}^2} - \xi \frac{\partial^3 \hat{w}_s^{K+1}}{\partial \hat{x}^3} = \alpha \hat{q}_{elec}(V^{K+1}, \hat{w}_s^{K+1}). \tag{35}$$

Now, for the investigation of a small value of δV , $\psi(\hat{x})$ should be small enough; therefore, using the calculus of variation theory and Taylor’s series expansion about \hat{w}_s^K , and applying the truncation to its first order for a suitable value of δV , it is possible to obtain desired accuracy. So, the linearized equations to calculate $\psi(\hat{x})$ are:

$$\frac{\partial^4 \psi}{\partial \hat{x}^4} - \alpha_1 \frac{\partial^6 \psi}{\partial \hat{x}^6} + \alpha_2 \frac{\partial^2 \psi}{\partial \hat{x}^2} - \xi \frac{\partial^3 \psi}{\partial \hat{x}^3} - \alpha \frac{\partial \hat{q}_{elec}}{\partial \hat{w}_s^K} \psi - \alpha \frac{\partial \hat{q}_{elec}}{\partial V} \delta V = 0. \tag{36}$$

The expansion theory is used to solve the above equation (Younis and Nayfeh 2003):

$$\psi(\hat{x}) = \sum_{j=1}^N a_j \varphi_j(\hat{x}), \tag{37}$$

where φ_j is the j th free vibration mode shape of the CNT. Substituting Eq. (37) into Eq. (36), multiplying both sides by φ_i and applying the Galerkin method, we have:

$$\sum_{j=1}^N K_{ij} a_j = F_i, \quad i = 1, \dots, n, \tag{38}$$

where $K_{ij} = K_{ij}^m + K_{ij}^f - K_{ij}^e$ and F_i are:

$$K_{ij}^m = \int_0^1 \varphi_i \varphi_j^{iv} d\hat{x} - \alpha_1 \int_0^1 \varphi_i \varphi_j^{vi} d\hat{x},$$

$$K_{ij}^f = \alpha_2 \int_0^1 \varphi_i \varphi_j'' d\hat{x} - \xi \int_0^1 \varphi_i \varphi_j''' d\hat{x}, \tag{39}$$

$$K_{ij}^e = \alpha \frac{\partial \hat{q}_{elec}}{\partial \hat{w}_s^K} \int_0^1 \varphi_i d\hat{x}, F_i = \alpha \frac{\partial \hat{q}_{elec}}{\partial V} \delta V \int_0^1 \varphi_i d\hat{x}.$$

Table 1 The comparison of the static pull-in voltage of CNTs

Boundary condition	Length scale (nm)	Fakhrabadi et al. (2013)	Present
C–F	0.1	0.43	0.41
	0.4	0.64	0.62
	0.5	0.72	0.71
C–C	0.1	6.00	6.12
	0.4	7.20	7.36
	0.5	7.80	7.73

3.2 Dynamic analysis

To solve the dynamic behaviour of the CNTs conveying fluid under DC voltage, the expansion theory is applied to Eq. (31) as follows (Karniadakis et al. 2006):

$$w_d(\hat{x}, \hat{t}) = \sum_{j=1}^N \varphi_j(\hat{x}) q_j(\hat{t}). \tag{40}$$

Next, substituting Eq. (40) into Eq. (31), multiplying both sides by φ_i and applying the Galerkin method lead to:

$$\sum_{j=1}^N M_{ij} \ddot{q}_j(\hat{t}) + \sum_{j=1}^N C_{ij} \dot{q}_j(\hat{t}) + \sum_{j=1}^N K_{ij} q_j(\hat{t}) = F_i, \tag{41}$$

where M, K, C and F are mass, stiffness, damping matrices and the force vector, respectively, and are defined as follows:

$$M_{ij} = \gamma \int_0^1 \varphi_i \varphi_j d\hat{x},$$

$$K_{ij} = \int_0^1 \varphi_i''' \varphi_j d\hat{x} + \alpha_2 \int_0^1 \varphi_i''' \varphi_j d\hat{x} - \alpha_1 \int_0^1 \varphi_i^{vi} \varphi_j d\hat{x} - \xi \int_0^1 \varphi_i''' \varphi_j d\hat{x},$$

$$C_{ij} = \beta \int_0^1 \varphi_i' \varphi_j d\hat{x} + \zeta \int_0^1 \varphi_i \varphi_j d\hat{x} - \delta \int_0^1 \varphi_i'' \varphi_j d\hat{x},$$

$$F_i = \alpha \int_0^1 \varphi_i \hat{q}_{elec}(V, \hat{w}) d\hat{x}. \tag{41}$$

Due to the complexity of the self-excited nonlinear Eq. (41), this equation is solved step by step in the time domain. In other words, at each discrete time step, the nonlinear forcing vectors are calculated based on the results of the previous step. In this method, if the time steps are sufficiently small, acceptable results can be obtained.

4 Numerical results

This section presents the results obtained from Eq. (41).

4.1 Validation

To validate our results, two verification procedures have been performed. In Table 1, static pull-in voltage is compared with the results of Seyyed Fakhrabadi et al. (2013) and in Table 2 dynamic behaviour is compared with the results of Dai et al. (2015). Our results are in good agreement with those in the literature.

In the next sections, we discuss the effects of Kn and the slip boundary condition on the dynamic and pull-in instability of the CNTs for C–F and C–C boundary conditions using the SGT. The material and geometrical properties of CNTs are as follows (Fakhrabadi et al. 2013): CNT Young’s modulus $E = 1$ TPa; shear modulus $G = 0.4$ TPa and mass density of CNT $\rho_c = 2300$ kg m⁻³; gap distance $G_0 = 4$ nm; radius $R = 0.6785$ nm; thickness $h = 0.34$ nm; length $L = 50$ nm and length scale parameters of SGT $l_0 = l_1 = l_2 = 0.2$ nm; fluid mass density and viscous fluid are $\rho_f = 1.169$ kg m⁻³ and $\mu = 3 \times 10^{-7}$ Pa s, respectively (Kaviani and Mirdamadi 2012; Cengel 2007).

4.2 Pull-in instability

The static pull-in voltage of cantilever and doubly clamped CNTs for no flow condition ($u = 0$), under continuum flow and with slip flow regimes, is shown in Figs. 2 and 3, respectively. As it was expected for no flow condition, the static pull-in voltage of the C–C CNT is higher than for the C–F CNT due to the stiffer structure of C–C CNT. It follows from Fig. 2 that the fluid flow increases the static pull-in voltage of the C–F CNT and decreases in the C–C CNT. This opposite effect of the fluid versus the axial force results from the fluid flow through the CNTs. For the cantilever

Table 2 Comparison of the dynamic behaviour of CNTs ($E = 7.56$ GPa, $G = 2.9$ GPa, $l = 0$ μm , $\rho = 1000$ kg/m³, $\rho_m = 970$ kg/m³, $b = 150$ μm , $h = 50$ μm , $b_i = 67.9$ μm , $h_i = 22.6$, $L = 30$ nm)

Boundary condition	Flow speed	Dai et al. (2015)	Present
C–F	1	1.37	1.33
	2	1.56	1.53
	3	1.97	1.97
	4	2.72	2.98
C–C	1	8.25	8.19
	2	7.83	7.82
	3	7.07	7.13
	4	5.84	5.87

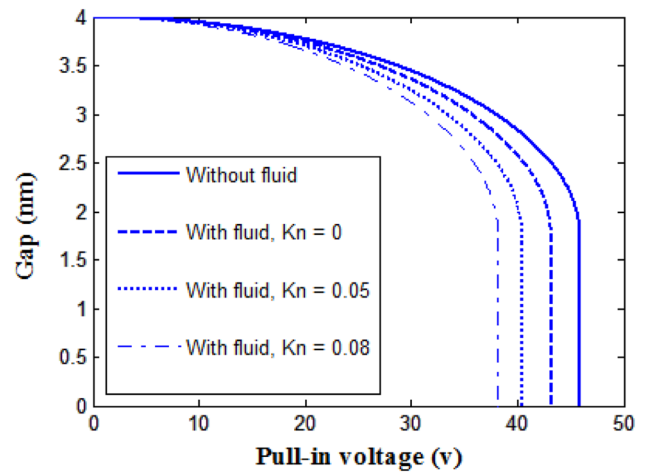


Fig. 2 The effect of Knudsen number on the static pull-in behaviours of C–C CNTs using the SGT

boundary conditions, the axial force remains tensile because of the free end. The tensile force increases the stiffness of the CNT. However, for doubly clamped CNTs, the clamped ends transform the axial force to the compressive force and thus reduce the stiffness (Fakhrabadi et al. 2014). When the flow regime passes from its continuum condition to the slip flow regime, the axial force produced by the fluid flow increases, therefore, the static pull-in voltage in the slip flow regime decreases more and increases more compared to continuum flow regime in C–C and C–F CNTs, respectively.

The effects of Kn on the dynamic pull-in voltage for three values of the flow speed ($u = 1, 2$ and 3) are shown for both C–C and C–F CNTs in Figs. 4 and 5, respectively. From Fig. 4, it can be concluded that increasing Kn causes a decrease of the pull-in voltage for different values of u and

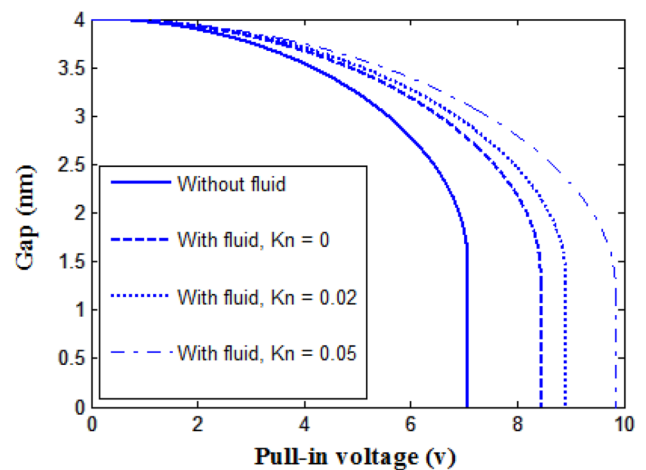


Fig. 3 The effect of the Knudsen number on the static pull-in behaviour of C–F CNTs using the SGT

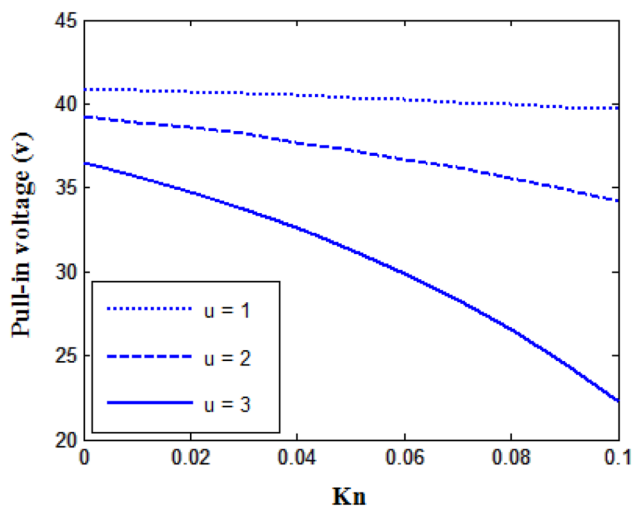


Fig. 4 The effect of the Knudsen number on the static pull-in of C–C CNTs for different values of flow speed

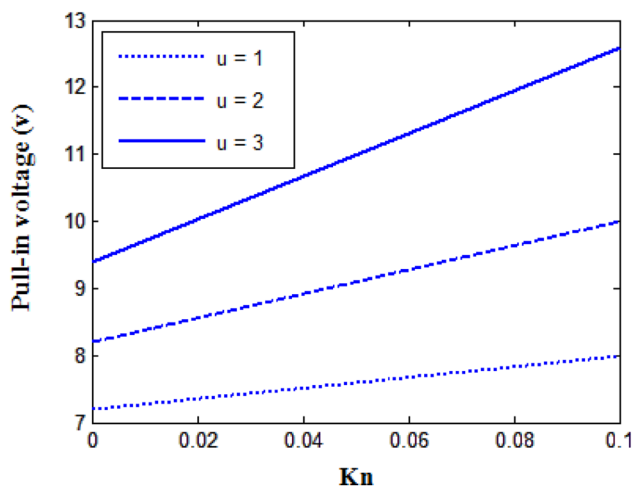


Fig. 5 The effect of the Knudsen number on the static pull-in behaviour of C–F CNTs for different values of flow speed

this decrease is more significant for larger values of u . Figure 5 shows that for the C–F CNT the Kn parameter has an opposite effect. Furthermore, these illustrations demonstrate that the effect of Kn on the dynamic pull-in voltage of the C–F CNT for different values of u is almost stable, whereas for the C–C CNT and larger values of u it is greater.

4.3 The instability regions

The stability boundaries for C–C and C–F CNTs are shown in Figs. 6 and 7, respectively. The diagrams are divided into two sub-regions (stable and unstable). As it can be seen from Fig. 6 for the C–C CNT case, when $V < 8.6$, buckling instability occurs due to the internal flow as u crosses the

boundary from the left side. When $8.6 < V < 41.2$, pull-in instability occurs when u crosses the boundaries from the left side, and finally for $V > 41.2$ the system is totally unstable for all values of the flow speed. Next, we conclude that when Kn increases the stable region decreases—this means that for the slip regime for constant voltage the system is unstable for smaller u than in the continuum regime and that the value of u which will make the system unstable is smaller as Kn increases. Note that for the C–C CNT the increase of Kn has almost no effect on the buckling instability boundary but decreases the pull-in instability boundary.

The instability and stability region diagram for the C–F CNT has a different shape compared to the diagram for the C–C CNT, as illustrated in Fig. 7. For the C–F CNT we have pull-in and flutter instabilities. Figure 7 shows that for a small value of V ($V < 7.1$) when u increases and crosses the boundary, it causes flutter instability in the system. Furthermore, for relatively large values of the applied voltage ($7.1 < V < 21.8$) the CNT is unstable when u is small (when u increases, the system will be stable and then unstable again). The effect of Kn is the same for the C–C CNT in which increasing Kn decreases the stable region. This means that the stable region for the slip regime is smaller than for continuum regime. Finally, when $V > 21.8$, for the slip regime pull-in instability of the system occurs for smaller u versus the continuum regime, and u becomes smaller as Kn increases. On the other hand, flutter instability occurs for smaller u , too.

As a closing remark, notice that in the slip regime the effect of the flow speed on the stability and the instability of the system is greater than for continuum regime, and this effect is more pronounced as Kn increases. This means that for smaller change of u one can control stability of the system in the slip regime.

5 Conclusions

In this study, we investigated the static pull-in instability and the dynamics of CNTs conveying fluid assuming both the continuum and the slip flow regimes based on the SGT. Furthermore, we considered different boundary conditions on CNT, i.e. doubly clamped and cantilever boundary conditions. We studied the effect of the Kn parameter on the static pull-in voltage and we observed that the fluid flow increases and decreases the stiffness of the C–F and C–C CNTs, respectively, which results in greater and smaller static pull-in voltage. Moreover, the slip flow regime decreases more the pull-in voltage for C–C CNTs and increases it more for C–F CNTs compared to the continuum flow regime. In the slip flow regime these effects were magnified as Kn increased.

Fig. 6 The instability region in the (u, V) plane for a C–C CNT in different regimes

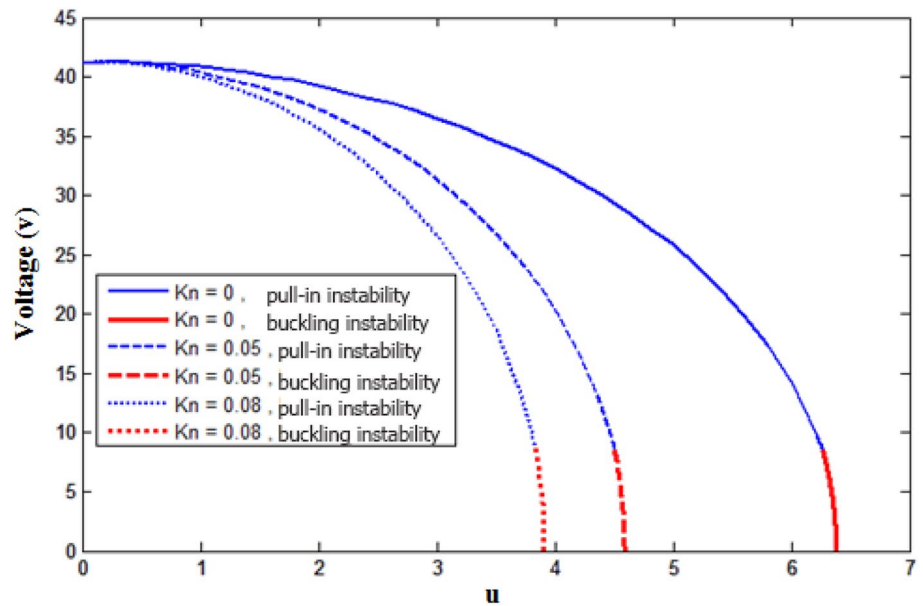
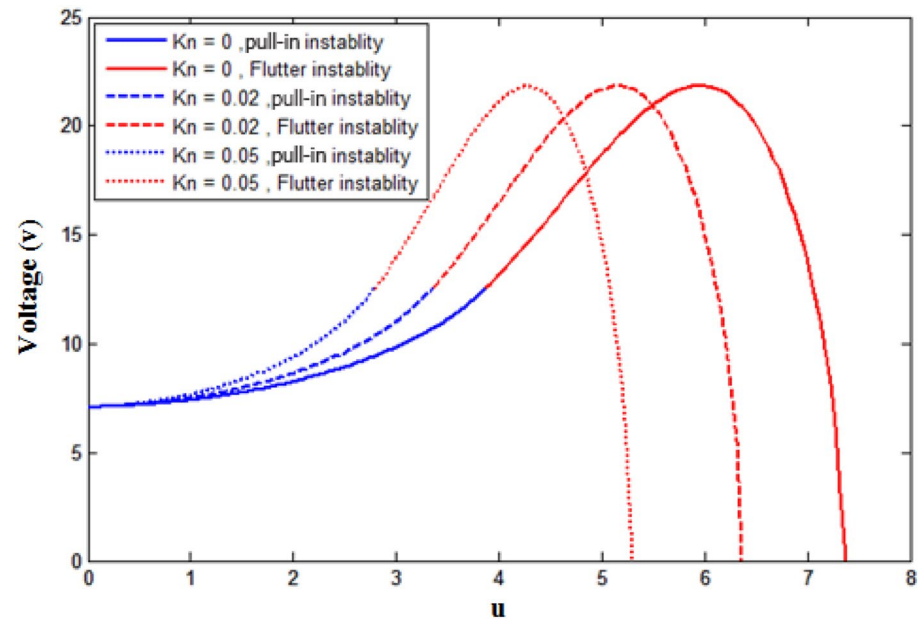


Fig. 7 Instability region in the (u, V) plane for a C–F CNT in different regimes



We studied the effects of Kn on the dynamic and stability regions of CNTs and we obtained the following results:

- In the case of C–C CNT, the dynamic pull-in voltage of the slip flow regime is greater than in the continuum regime.
- The increase of Kn results in higher increase of the pull-in voltage, especially for greater speed of the flow regime.
- As Kn increases, the stability region becomes smaller, which means that the instability of the system will occur for smaller u compared to the continuum flow regime.

For C–F CNTs, the dynamic pull-in voltage decreases as the flow regime changes from continuum to slip. Similar to C–C CNTs, Kn has the same effect on the stability region in which for the slip flow regime smaller changes of speed could result in instable or stable versus continuum flow, and as Kn increases this interval is smaller.

Acknowledgements The third author acknowledges the support of the National Science Centre, Poland, under Grant No. 2017/27/B/ST8/00351.

Open Access This article is distributed under the terms of the Creative Commons Attribution 4.0 International License (<http://creativecommons.org/licenses/by/4.0/>), which permits unrestricted use, distribution, and reproduction in any medium, provided you give appropriate credit to the original author(s) and the source, provide a link to the Creative Commons license, and indicate if changes were made.

References

- Beskok A, Karniadakis GE (1999) A model for flows in channels, pipes, and ducts at micro and nano scales. *Microscale Thermophys Eng* 3:43–77
- Cengel YA (2007) Heat and mass transfer: a practical approach, 3rd edn. McGrawHill, New York
- Chang WJ, Lee HL (2009) Vibration analysis of fluid-conveying double-walled carbon nanotubes based on nonlocal elastic theory. *J Phys Condens Matter* 21(11):115302
- Che G, Lakshmi BB, Fisher ER, Martin CR (1998) Carbon nanotubule membranes for electrochemical energy storage and production. *Nature* 393(6683):346
- Dai HL, Wang L, Ni Q (2015) Dynamics and pull-in instability of electrostatically actuated microbeams conveying fluid. *Microfluid Nanofluid* 18(1):49–55
- Dequesnes M, Rotkin SV, Aluru NR (2002) Calculation of pull-in voltages for carbon-nanotube-based nanoelectromechanical switches. *Nanotechnology* 13(1):120
- Dequesnes M, Tang Z, Aluru NR (2004) Static and dynamic analysis of carbon nanotube-based switches. *J Eng Mater Technol* 126(3):230–237
- Evans E, Bowman H, Leung A, Needham D, Tirrell D (1996) Biomembrane templates for nanoscale conduits and networks. *Science* 273(5277):933–935
- Fakhrabadi MMS, Rastgoo A, Ahmadian MT (2013) Dynamic behaviours of carbon nanotubes under dc voltage based on strain gradient theory. *J Phys D Appl Phys* 46(40):405101
- Fakhrabadi MMS, Rastgoo A, Ahmadian MT (2014) Carbon nanotube-based nano-fluidic devices. *J Phys D Appl Phys* 47(8):085301
- Ghazavi MR, Molki H (2018) Nonlinear analysis of the micro/nanotube conveying fluid based on second strain gradient theory. *Appl Math Model* 60:77–93
- Guo Y, Xie J, Wang L (2018) Three-dimensional vibration of cantilevered fluid-conveying micropipes—types of periodic motions and small-scale effect. *Int J Non Linear Mech* 102:112–135
- Hajnayeb A, Khadem SE (2012) Nonlinear vibration and stability analysis of a double-walled carbon nanotube under electrostatic actuation. *J Sound Vib* 331(10):2443–2456
- Iijima S (1991) Helical microtubules of graphitic carbon. *Nature* 354(6348):56
- Kahrobaiyan MH, Asghari M, Rahaeifard M, Ahmadian MT (2011) A nonlinear strain gradient beam formulation. *Int J Eng Sci* 49(11):1256–1267
- Karniadakis G, Beskok A, Aluru N (2006) *Microflows and nanoflows: fundamentals and simulation*, vol 29. Springer, New York
- Kaviani F, Mirdamadi HR (2012) Influence of Knudsen number on fluid viscosity for analysis of divergence in fluid conveying nanotubes. *Comput Mater Sci* 61:270–277
- Kaviani F, Mirdamadi HR (2013) Wave propagation analysis of carbon nano-tube conveying fluid including slip boundary condition and strain/inertial gradient theory. *Comput Struct* 116:75–87
- Kucaba-Piętal A (2004) Microchannels flow modelling with the micropolar fluid theory. *Tech Sci* 52(3):209–214
- Mirramezani M, Mirdamadi HR (2012a) Effects of nonlocal elasticity and Knudsen number on fluid–structure interaction in carbon nanotube conveying fluid. *Phys E* 44(10):2005–2015
- Mirramezani M, Mirdamadi HR (2012b) The effects of Knudsen-dependent flow velocity on vibrations of a nano-pipe conveying fluid. *Arch Appl Mech* 82(7):879–890
- Mirramezani M, Ghayour M, Mirdamadi HR (2013) Innovative coupled fluid–structure interaction model for carbon nano-tubes conveying fluid by considering the size effects of nano-flow and nano-structure. *Comput Mater Sci* 77:161–171
- Ouakad HM, Younis MI (2010) Nonlinear dynamics of electrically actuated carbon nanotube resonators. *J Comput Nonlinear Dyn* 5(1):011009
- Rahimi Z, Rezazadeh G, Sumelka W, Yang XJ (2017) A study of critical point instability of micro and nano beams under a distributed variable-pressure force in the framework of the fractional non-linear nonlocal theory. *Arch Mech* 69(6):413–433
- Rasekh M, Khadem SE, Tatari M (2010) Nonlinear behaviour of electrostatically actuated carbon nanotube-based devices. *J Phys D Appl Phys* 43(31):315301
- Shames IH (1962) *Mechanics of fluid*. U3, McGraw-Hill, New York, p 11
- Shokouhmand H, Isfahani AHM, Shirani E (2010) Friction and heat transfer coefficient in micro and nano channels filled with porous media for wide range of Knudsen number. *Int Commun Heat Mass* 37:890–894
- Talebian S, Rezazadeh G, Fathalilou M, Toosi B (2010) Effect of temperature on pull-in voltage and natural frequency of an electrostatically actuated microplate. *Mechatronics* 20:666–673
- Umeda M, Kishi A, Shironita S (2012) Fabrication of Pt nano-dot-patterned electrode using atomic force microscope-based indentation method. *Electrochim Acta* 63:251–255
- Wang L, Ni Q (2009) A reappraisal of the computational modelling of carbon nanotubes conveying viscous fluid. *Mech Res Commun* 36:833–7
- Wang L, Ni Q, Li M (2008) Buckling instability of double-wall carbon nanotubes conveying fluid. *Comput Mater Sci* 44:821–825
- Wang L, Hong Y, Dai H, Ni Q (2016) Natural frequency and stability tuning of cantilevered CNTs conveying fluid in magnetic field. *Acta Mech Solida Sin* 29(6):567–576
- Xu Z, Fang F, Gao H, Zhu Y, Wu W, Weckenmann A (2012) Nano fabrication of star structure for precision metrology developed by focused ion beam direct writing. *CIRP Ann Manuf Technol* 61(1):511–514
- Yamamoto H, Ohnuma A, Kozawa T, Ohtani B (2012) Location control of nanoparticles using combination of top-down and bottom-up nano-fabrication. *J Photopolym Sci Technol* 25(4):449–453
- Yoon J, Ru CQ, Mioduchowski A (2005) Vibration and instability of carbon nanotubes conveying fluid. *Compos Sci Technol* 65(9):1326–1336
- Younis MI, Nayfeh AH (2003) A study of the nonlinear response of a resonant microbeam to an electric actuation. *Nonlinear Dyn* 31:91–117
- Zhang Z, Liu Y, Zhao H, Liu W (2016) Acoustic nanowave absorption through clustered carbon nanotubes conveying fluid. *Acta Mech Solida Sin* 29(3):257–270
- Zhang YW, Zhou L, Fang B, Yang TZ (2017) Quantum effects on thermal vibration of single-walled carbon nanotubes conveying fluid. *Acta Mech Solida Sin* 30(5):550–556
- Zhen Y, Fang B (2010) Thermal–mechanical and nonlocal elastic vibration of single-walled carbon nanotubes conveying fluid. *Comput Mater Sci* 49(2):276–282

Publisher's Note Springer Nature remains neutral with regard to jurisdictional claims in published maps and institutional affiliations.